Upcycling of carrot waste into pectin-arabinogalactan and lignin-cellulose films via hydrothermal treatment, ultrafiltration/diafiltration, and casting

Ramos-Andrés, M.; Hu, L.; Grénman, H.; Xu, C.; García-Serna, J.

Published in:
Journal of Environmental Chemical Engineering

DOI:
10.1016/j.jece.2024.112645
10.1016/j.jece.2024.112645

Published: 03/06/2024

Document Version
Final published version

Journal of Environmental Chemical Engineering 12 (2024) 112645

Contents lists available at ScienceDirect

Journal of Environmental Chemical Engineering

journal homepage: www.elsevier.com/locate/jece

Upcycling of carrot waste into pectin-arabinogalactan and lignin-cellulose films via hydrothermal treatment, ultrafiltration/diafiltration, and casting

Marta Ramos-Andrés [a], Liqiu Hu [b], Henrik Grénman [c,*], Chunlin Xu [b,*], Juan García-Serna [a,*]

[a] Pressure Technologies group (PressTech), Instituto de Bioeconomía de la Universidad de Valladolid (BioEcoUVa), Department of Chemical Engineering and Environmental Technology, School of Industrial Engineering, Universidad de Valladolid, Valladolid 47011, Spain
[b] Johan Gadolin Process Chemistry Centre, Laboratory of Natural Materials Technology, Åbo Akademi University, Turku 20500, Finland
[c] Johan Gadolin Process Chemistry Centre, Industrial Chemistry and Reaction Engineering, Åbo Akademi University, Turku 20500, Finland

ARTICLE INFO

Keywords:
Food-packaging
Hemicellulose
Homogalacturonan
CNFs
Purification
Biorefinery

ABSTRACT

Discarded carrots were repurposed to produced bio-based films through a pilot-scale hydrothermal treatment of the pulp. The process, conducted at 140 °C and 180 °C using single and multiple flow-through reactors, successfully extracted high molecular weight pectin-containing arabinogalactan (P-AG). Separation and purification through ultrafiltration and diafiltration yielded fractions with molecular weights ranging from 3.48 to 102.75 kDa. The solid residue from the hydrothermal process was subjected to mechanical treatments to obtain lignin-containing cellulose nanofibers (L-CNFs). Comparative analysis showed the P-AG film possessed superior oxygen barrier properties (67.73 vs. 239.83 $cm^3 \cdot \mu m/m^2/kPa/day$), while the L-CNFs film displayed higher tensile strength (7.74 vs. 3.14 MPa). Combining both fractions revealed that L-CNFs could be incorporated at percentages exceeding 15% (w/w) without compromising the P-AG-based film's integrity, resulting in a 57.5% increase in water contact angle (125.8°). In examining P-AG samples, a higher molecular weight reduced oxygen permeability by 14.6% (41.14 $cm^3 \cdot \mu m/m^2/kPa/day$) but increased the water vapor permeability by 11.4% ($2.78 \cdot 10^{-10}$ $g \cdot m/m^2/s/Pa$). Tensile strength showed a 150.9% increase at lower molecular weights and higher pectin content (2.84 MPa), attributed to arabinogalactan's pronounced branching. Elongation increased by 157.9% at higher arabinogalactan content (15.28%). This study achieved a groundbreaking milestone by obtaining purified fractions of P-AG and L-CNFs from carrot waste, demonstrating promising film properties suitable for food packaging applications.

1. Introduction

Carrots (*Daucus carota* L.) stand as crucial cultivated vegetables globally, yielding approximately 36 million tons annually [1]. However, in processing plants, around 20–25% is discarded due to factors such as breakage, incorrect shape, color, or size, leading to substantial waste [2]. Carrot pulp, a byproduct in the juice industry, contributes to this waste, comprising 30–50% of the initial carrot mass [3].

The high moisture content and organic load of carrot waste pose challenges for efficient valorization, resulting in a substantial amount ending up in landfills. The waste, however, contains valuable components, with free sugars and carotenoids being predominant, alongside biopolymers like cellulose, lignin, hemicellulose (arabinogalactan), and pectin [4].

Prior research has primarily focused on fermenting sugars for ethanol [5,6], 2,3-butanediol [7], and butanol [8], as well as extracting carotenoids using environmentally friendly methods [9]. Some studies propose a more comprehensive valorization by fractionating the waste into carotenoids, fiber, and sugars [10,11]. However, limited attention has been given to bioplastic production from carrot waste, with a predominant focus on cellulose content, despite the other biopolymers (hemicellulose, pectin and lignin) collectively comprising up to double the cellulose content [4]. Idrovo Encalada et al. (2016) produced films based on commercial pectin to which they added carrot fibers [12]. The carrot fibers had antioxidant effect as well as good mechanical properties. Varanasi et al. (2018) and Amoroso et al. (2022) produced nanofibers from carrot waste, demonstrating that it is a more economical process than producing them from wood [3,13]. Perotto et al. (2020) cast films from carrot powder and formic acid [14]. The films were composed mostly of cellulose and pectins, and their properties were

* Corresponding authors.
E-mail addresses: henrik.grenman@abo.fi (H. Grénman), chunlin.xu@abo.fi (C. Xu), juan.garcia.serna@uva.es (J. García-Serna).

https://doi.org/10.1016/j.jece.2024.112645
Received 6 November 2023; Received in revised form 13 March 2024; Accepted 28 March 2024
Available online 29 March 2024

highly dependent on moisture. Sogut and Calmak (2020) prepared chitosan-based films to which they added carrot fibers from the juice industry and microcrystalline cellulose for comparison [15]. Both additives improved the tensile properties and thermal stability of the films.

In our previous work, we proposed a complete valorization process for discarded carrots, involving separation of juice and pulp. Carotenoids and sugars from the juice were valorized by microencapsulation and fermentation [16], while the pulp underwent hydrothermal treatment for the extraction hemicelluloses and pectins [4,17]. As the arabinogalactan hemicelluloses from carrot are covalently bonded to the homogeneous part of pectins (homogalacturonan) [18], both were co-extracted. Subsequent purification steps yielded fractions of pectin-containing arabinogalactan (P-AG) with varying molecular weights [19].

Hemicelluloses and pectins can be the basis of biomaterials [20]. They are known for their biocompatibility, biodegradability, and non-toxicity, promising avenues for sustainable production. However, the strong inter- and intramolecular hydrogen bonds in cellulose, hemicellulose, pectin and lignin limit their direct transformation into bioplastics [21]. Fractionation becomes essential for conditioning and blending these biopolymers in desired proportions, offering the advantages of polymer blending (simplicity, lack of chemical modification, and high biodegradability) [22].

Hemicelluloses and pectins are extracted from biomass through methods like acid hydrolysis, hydrothermal treatment, alkaline treatment, and organic solvents. Among these methods, hydrothermal treatment stands as the least aggressive and most environmentally friendly, utilizing only biomass and water. To ensure their use in biomaterials, these extracted biopolymers require not only adequate molecular weight but also high purity, achievable through environmentally friendly processes like ultrafiltration (UF) and diafiltration (DF) [19].

While films from pectins and hemicelluloses have been studied, there is a notable gap in exploring arabinogalactan hemicellulose found in carrots. Regarding arabinogalactan films from other sources, Cheribi et al. (2019) valorized the mucilage of *Opuntia ficus-indica* to obtain casting films that had acceptable properties to act as coating material for foodstuffs or paper/cardboard packaging [23]. Oliveira et al. (2019) produced arabinogalactan films from leaves of *Pereskia aculeata* Miller by casting in combination with glycerol [24]. The films were flexible, with smooth surfaces without cracks, and of dark color. Clen et al. (2021) produced casting films based on cellulose nanocrystals to which three types of hemicelluloses were incorporated: arabinogalactan, galactomannan or glucomannan [25]. The arabinogalactan films proved to be the most brittle due to the more branched character of this hemicellulose compared to the others, as already demonstrated in other studies [20].

Recent studies continue to investigate the production of films using hemicelluloses other than arabinogalactan, as well as pectins. Ren et al. (2022) prepared pectin-based films improving their mechanical properties through the introduction of Ca^{2+} ions, increasing the tensile strength from 5.9 to 12.7 MPa [26]. Similar to the present work, Mugwagwa and Chimphango (2022) produced films by blending hemicellulose, pectin, and nanocellulose enriched with polyphenols [27]. The pectin-based films (>50%) had higher tensile strength than the hemicellulose-based films. However, hemicellulose-based films (>50%) had higher elongation than pectin-based films.

Additionally, attention has been directed towards the production of lignin-containing cellulose nanofibers (L-CNFs) for the formation of bioplastics. L-CNFs, particularly from waste biomass, offer advantages such as less chemically altered lignin, cellulose with increased hydrophobicity, and environmental sustainability. Recent studies have employed L-CNFs as reinforcing agents in polylactic acid (PLA) films, demonstrating improved mechanical properties and enhanced biodegradability of PLA [28]. The incorporation of L-CNFs has also proven effective in providing antioxidant and UV blocking properties, contributing to the overall performance of the films [29]. However, an excessive content of L-CNFs could result in poorer barrier properties.

The present work aligns with these advancements, aiming to valorize discarded carrot pulp through the production of films. Two key fractions recovered from the pulp, namely purified high molecular weight P-AG and L-CNFs, are explored. This study presents a unique contribution by addressing multiple aspects such as 1) film production from new fractions derived from carrot waste (P-AG and L-CNFs) alone and in combination, 2) film production from hydrothermally extracted biopolymers subjected to multiple stages of UF/DF, and 3) utilization of hemicelluloses naturally covalently bound to pectins. The films exhibit desirable properties for application in food packaging, featuring notably high surface hydrophobicity. In aligning with current trends in film production from lignocellulosic materials, this study adds a novel dimension by utilizing specific fractions derived from discarded carrot pulp, contributing to the broader landscape of sustainable bioplastics.

2. Materials and methods

2.1. Raw material preparation and characterization

The discarded carrots were provided by Muñozval S.L. (Valladolid, Spain) and stored under controlled conditions in a cool, dry, and dark environment for short durations to prevent alterations in their properties. Processing involved the use of a juice extractor (Moulinex ZU5008 Infinity Press Revolution), resulting in the separation of pulp and juice. Approximately 0.545 kg of pulp was obtained from every 1 kg of carrots.

The discarded carrots were fully characterized according to the standardized methods by the National Renewable Energy Laboratory (NREL), as detailed in our previous work [4]. Initially, the moisture content of carrot pulp was determined to express composition on a dry basis. Subsequently, the dried discarded carrot pulp underwent two consecutive Soxhlet extractions, employing water and hexane in separate steps. These extractions facilitated the quantification of polar and apolar extractives, respectively. Protein content was determined applying the Kjeldahl method. Polysaccharides (cellulose, hemicellulose, pectin) and lignin were determined by two-step acid hydrolysis process, distinguishing acid-insoluble (acid-insoluble lignin and ash) and acid-soluble (acid-soluble lignin, cellulose, hemicellulose, and pectin) fractions. Acid-insoluble lignin and ash were determined gravimetrically, with ash measured post-oxidation at 550 °C. Acid-insoluble lignin was quantified using UV-Vis spectroscopy. In the second step of the acid hydrolysis, cellulose, hemicellulose and pectin were hydrolyzed to obtain the monomers, subsequently analyzed via HPLC according to Section 2.4.

2.2. Hydrothermal treatment

The extraction of hemicelluloses and pectins, along with a portion of free sugars, was executed through a hydrothermal treatment in a pilot plant comprising five flow-through reactors in series. The detailed operation of this plant, patented [30], was previously elucidated in our work [17]. Each reactor operates semicontinuously, with biomass initially loaded into through a cartridge. A constant circulation of water at the desired conditions traversed the reactors from top to bottom. These reactors, operable in series or individually, facilitated cyclic operation by connecting the outlet of the last reactor to the inlet of the first, enabling prolonged operation with large quantities of raw material (kilograms). The operation of the reactors in parallel instead of in series is currently not envisaged because the individual flow in each reactor is not controlled, but only the total flow.

In this study, three extraction experiments were conducted, one with a single reactor and two with multiple reactors. Before initiating any experiment, a cold pressure test ensured the absence of leaks or clogs. A constant flow of 10 L/h of fresh water circulated in bypass mode through the pilot plant until it reached the desired extraction temperature and pressure, passing through two concentric tube heat exchangers and an

electric heater. The reactors, each with a 2 L volume, were filled with the desired amount of biomass and fresh water and were preheated to 90°C by means of heating resistors located on the wall. Once the desired temperature and pressure were attained in the plant, the 10 L/h fresh water passed through the reactor/s. The hydrothermal extract, after passing through three heat exchangers for cooling and energy recovery, passed through a valve that keeps the plant pressurized. The hydrothermal extract was collected in a tank. Sample ports at the plant and reactors outlets facilitated monitoring.

Three operating conditions were used: 25 min at 140 °C (E1), 45 min at 140 °C (E2), and 30 min at 180 °C (E3), selected based on previous results [4]. E1 utilized a single reactor, while E2 and E3 involved a total of seven reactors operating in cycles of three reactors working in series. Extractions lasted 150 min (E2) and 100 min (E3), with individual reactor operation time of 45 min (E2) and 30 min (E3). The operating pressures, up to 15 barg, maintained water in liquid state. Discarded carrots, ranging from 1.62 kg (1 reactor) to 11.3 kg (7 reactors), were treated in each experiment. The chemical composition and molecular weight distribution of hydrothermal extracts were determined according to Section 2.4.

The residual pulp after E2 extraction (140 °C, 45 min) was collected from the first reactor at the end of the extraction. This sample, subjected to the longest extraction time and moderate temperature, was washed, freeze-dried, and characterized per the methods outlined in Section 2.1.

2.3. Ultrafiltration and diafiltration

The three hydrothermal extracts (E1, E2 and E3) underwent several stages of UF and DF utilizing membranes for the concentration, separation, and purification of the pectin-containing hemicelluloses. Three UF membranes were employed, including two Pellicon 2 Mini Biomax polymeric membranes, flat sheet configuration, made of polyethersulfone, with molecular weight cut-off (MWCO) of 30 and 10 kDa, and a filtration area of 0.1 m^2. The third membrane, a 1 kDa Prep Scale-TFF polymeric membrane, featured a spiral wound configuration made of regenerated cellulose, with a filtration area of 0.23 m^2.

Initiating with microfiltration to eliminate particles > 50 μm, the concentration was subsequently increased by reducing the feed volume by 80% (v/v) during each UF stage. After UF, separation and purification of retained biopolymers occurred through several cycles of DF with water. Each DF cycle involved adding water equal to the feed volume and ultrafiltrating, ensuring the removal of free sugars, by-products, and low molecular weight hemicelluloses and pectins over at least five cycles. The transmembrane pressure was maintained within the range 2–3.5 bar via a manually adjustable valve on the retentate side, with a feed flow rate of approximately 4.8 L/m^2/min.

Fig. 1 illustrates the schematic diagram of the UF and DF schemes applied to E1, E2 and E3 extracts. E1 underwent UF/DF with the 30 kDa membrane, with the 30 kDa diafiltrated retentate recovered as the purified fraction (E1-R30). E2 underwent UF/DF sequentially with the 10 kDa and 30 kDa membranes, resulting in the recovery of the 30 kDa retentate and the 30 kDa permeate as distinct products (E2-R30 and E2-P30). E3, due to its already high concentration after the 10 kDa membrane, skipped UF with the 30 kDa membrane, undergoing UF/DF with the 10 and 1 kDa membranes and DF with the 30 kDa membrane. Recovered products included the 30 kDa diafiltrated retentate, DF waters from the 30 kDa membrane, and the 1 kDa diafiltrated retentate (E3-R30, E3-DF30, and E3-R1). Liquid samples were analyzed for composition and molecular weight according to Section 2.4, and subsequently, dried in accordance with Section 2.5.

2.4. Analysis of the liquid samples

The liquid samples containing pectin-containing hemicelluloses were analyzed prior to drying. The chemical composition was assessed using high-performance liquid chromatography (HPLC), following the method outlined by Ramos-Andrés et al. (2020) [4]. A SUGAR SH-1011 Shodex column was employed, maintaining a column temperature of 50 °C. The mobile phase consisted of 0.01 N sulfuric acid at a flow rate of 0.8 mL/min. Carbohydrates, uronic acids, aldehydes, and organic acids were identified and quantified using a Waters IR 2414 detector. Degradation compounds, namely 5-HMF and furfural, were determined with a Waters dual λ absorbance detector 2487 (210 and 254 nm). Concentration of hemicelluloses and pectins was determined through standardized hydrolysis, breaking down the biopolymers into monomeric units. The composition was determined by the difference in monomer concentration before and after hydrolysis. Calibration standards included sucrose (99%), galacturonic acid (97%), glucose (99%), galactose (99%), fructose (99%), arabinose (99%), glycolaldehyde (99%), formic acid (98%), acetic acid (98%), levulinic acid (98%), acrylic acid (99%), 5-hydroxymethylfurfural (99%), and furfural (99%), all sourced from Merck.

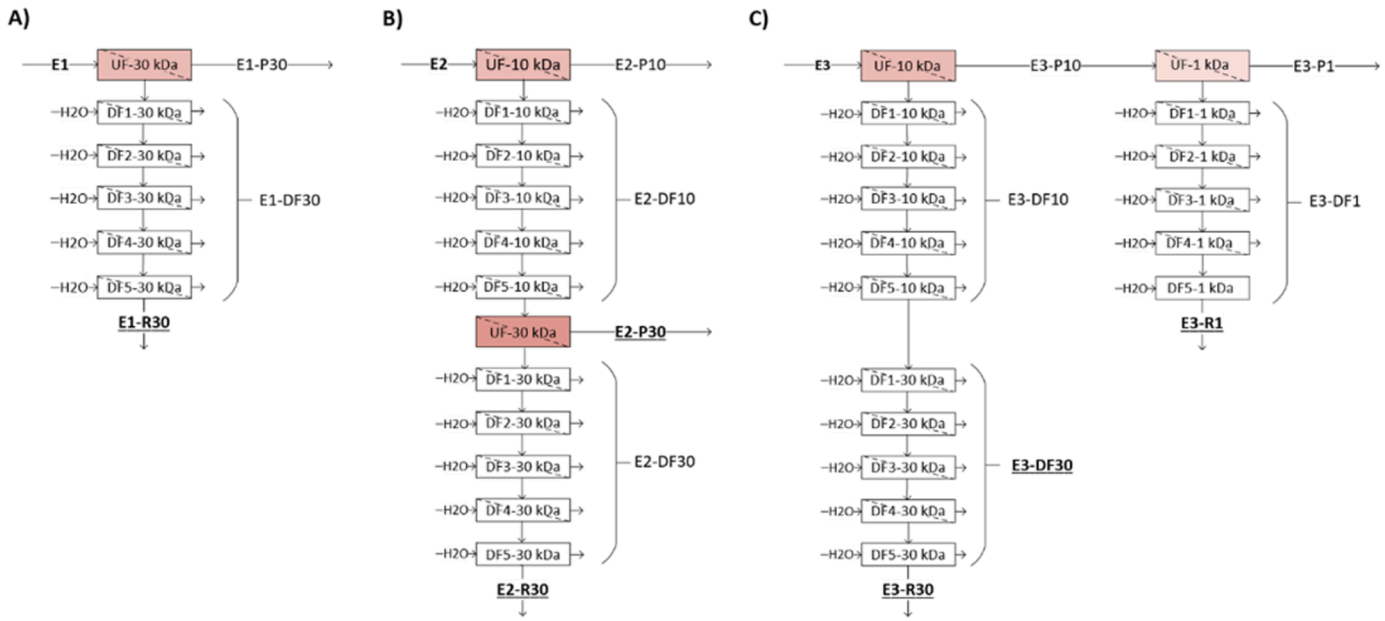

Fig. 1. Configuration of membranes for ultrafiltration and diafiltration treatments applied to hydrothermal extracts (E1, E2 and E3).

The molecular weight of the pectin-containing hemicellulose samples prior to drying was assessed using size exclusion chromatography (HPLC-SEC), following the method detailed by Ramos-Andrés et al. (2020) [4]. A GPC column (SB-803 HQ; Shodex) with a guard column (SB-G; Shodex) was maintained at 35 °C. The mobile phase comprised $NaNO_3$ 0.1 M + NaN_3 0.02% in Milli-Q water, with a flow rate of 0.5 mL/min. The molecular weight distribution of hemicelluloses and pectin was determined with a Waters IR 2414 detector. Calibration utilized a curve calculated from 5 pullulan standards (STANDARD P-82; Shodex) dissolved in Milli-Q water, covering a weight-average molecular weight range from 6.1 to 113 kDa.

2.5. Drying of the purified fractions and the residual pulp

Freeze drying and spray drying methods were employed to ensure the shelf stability of the purified samples of pectin-containing hemicelluloses, as well as for the residual pulp sample. The residual pulp from one of the reactors of extraction E2 was freeze-dried due to its solid nature (non-pumpable for spray drying). Similarly, sample E1-R30 was freeze-dried since it was obtained in lower quantity, resulting from the extraction conducted with only one reactor. The freeze drying process involved overnight storage at −25°C, followed by freeze drying under vacuum (0.180 mbar) for 96 hours, utilizing a Telstar Lyoquest −55 unit with a condenser temperature of −50 °C.

For the remaining purified products (E2-R30, E2-P30, E3-R30, E3-DF30, and E3-R1), obtained from the extraction with seven reactors, spray drying was employed. A Mobile Minor spray dryer with a rotary atomizer from Gea Niro was utilized for this purpose. Liquid purified products were pumped using a peristaltic pump (Watson-Marlow 520) at a flow rate of approximately 1 L/h, with a nozzle pressure of 6 barg. The inlet air temperature was set at 160 °C, while the outlet air temperature ranged between 90–95 °C. The resulting solid products were used to produced films following the procedures outlined in Sections 2.6 and 2.7.

2.6. Lignin-containing cellulose nanofibers preparation

The freeze-dried residual pulp from the E2 extraction underwent several treatments to yield a suspension of L-CNFs. Initially, ball milling was conducted using a Retsch PM100 ball mill, operating for 4 hours in 1-minute intervals with 15-minute breaks to prevent sample overheating. Subsequently, the fibers underwent hydration through overnight magnetic stirring in water, resulting in a suspension concentration of 0.4% w/v. Following hydration, the suspension underwent high-pressure homogenization (ATS-100D) through 2 cycles at 200 bar and 10 cycles at 1000 bar.

Optical microscope images of the residual pulp before and after high-pressure homogenization were captured using a Nikon microscope, while transmission electron microscopy (TEM) images were acquired with a JEM-1400 PLUS TEM microscope (JEOL Ltd., Japan) in bright field mode, operating at an accelerating voltage of 80 kV.

2.7. Preparation of the films by casting

Aqueous blends of purified P-AG samples, L-CNFs, and glycerol were prepared for film formation based on the specified compositions detailed in Table 1. Glycerol, employed as a plasticizer and sourced by Merck, was utilized at a consistent percentage across all films. Initially, films were prepared using a single type of material. Film A was formulated with a P-AG sample (E3-R30), while film Z was centered around the L-CNFs sample derived from the E2 extraction. Subsequently, films were generated by combining the two materials (E3-R30 and L-CNFs) in varying proportions. These composite films, denoted AZ-1, AZ-2, AZ-5, AZ-15, and AZ-25 (representing 1–2-5–15-25% w/w of L-CNFs, respectively), aimed to explore the impact of L-CNFs concentration on film properties.

Table 1
Composition of the films.

Film	P-AG sample	P-AG (% w/w)	L-CNFs (% w/w)	Glycerol (% w/w)
A	E3-R30	65	0	35
Z	-	-	65	35
AZ-1	E3-R30	64	1	35
AZ-2	E3-R30	63	2	35
AZ-5	E3-R30	60	5	35
AZ-15	E3-R30	50	15	35
AZ-25	E3-R30	40	25	35
BZ-1	E1-R30	64	1	35
CZ-1	E2-R30	64	1	35
DZ-1	E2-P30	64	1	35
EZ-1	E3-DF30	64	1	35
FZ-1	E3-R1	64	1	35

P-AG: pectin-containing arabinogalactan, L-CNFs: lignin-containing cellulose nanofibers.

Concluding the film production phase, films with a consistent L-CNFs content (1% w/w) and diverse P-AG samples were produced to investigate the influence of P-AG sample composition and molecular weight. This set included films BZ-1 (E1-R30), CZ-1 (E2-R30), DZ-1 (E2-P30), EZ-1 (E3-DF30), and FZ-1 (E3-R1). The systematic variation in film compositions allowed for a comprehensive examination of the interplay between P-AG and L-CNFs in influencing film characteristics.

The preparation of the blends commenced by determining the appropriate volume of L-CNFs suspension (0.4 w/v %) based on the desired content for each film (Table 1). Once the volume was established, the prescribed amount of P-AG solid sample was added, supplemented with water if necessary, to achieve a total volume of approximately 157 mL. The blend underwent magnetic stirring and was heated at 40–50°C in a thermostated bath for 3 hours. Subsequently, the mixture was allowed to reach room temperature, continuing magnetic stirring overnight. The designated quantity of glycerol was dissolved in 3 mL of water and added to the mixture. The final blend underwent further magnetic stirring at 40–50°C in a thermostated bath for an additional 3 hours. Ultimately, the prepared samples were poured into Petri dishes (diameter 13.5 cm, VWR) and positioned in a ventilated oven at 40 °C for approximately 6 hours. Following this initial drying phase, the films underwent further drying and were stored in a room conditioned at 23 °C and 50% relative humidity (RH) until characterization. This systematic approach ensured uniform film preparation and consistent conditions for subsequent analyses.

2.8. Characterization of the films

The film thickness was determined using a Lorenz Wetter paper thickness meter (L&M micrometer SE250, Sweden) at 10 randomly selected positions across the film. The mean value derived from these measurements was employed in subsequent calculations. The precision of the measurements was maintained at ± 1 μm. The thickness data served as a critical parameter for the computation of permeability values.

Water vapor permeability (WVP) was assessed gravimetrically in accordance with the ASTM standard E96/E96M-05. The desiccant method was applied, involving the placement of anhydrous $CaCl_2$ (Honeywell Fluka™) in a dish covered with the test specimen, with edges sealed using molten wax. This assembly was introduced into a climate-controlled chamber set at 23°C and 90% RH for a duration of 4 days. The film's top side was exposed to the conditioned atmosphere. The water vapor transmission rate (WVTR) across the specimen was computed by measuring the increase in the assembly's weight during the analysis period, with the average value reported in $g/m^2 \cdot h$. WVP was then determined by multiplying WVTR by the film thickness and dividing by the partial water vapor pressure, expressing the measurements in $(g \cdot m)/(m^2 \cdot s \cdot Pa)$. Prior to characterization, the films were conditioned at 23 °C and 50% RH.

The oxygen transmission rate (OTR) was assessed in accordance with ASTM F1927, utilizing an oxygen permeability analyzer equipped with a coulometric sensor (Mocon Ox-Tran 2/21 MH/SS) under controlled conditions (23 °C, 50% RH). The oxygen concentration was meticulously recorded throughout the analysis duration, and OTR was quantified in cm^3STP/m^2·day. Oxygen permeability (OP) was subsequently determined by multiplying OTR by the film thickness and dividing by the partial pressure of oxygen, presenting the measurements in $(cm^3STP·\mu m)/(m^2·kPa·day)$.

Contact angle measurements were conducted using an optical goniometer (CAM 200, KSV NIMA, Biolin Scientific Oy) and One Attension Theta 1.4 software. Drops of 18.2 MΩ type-1 deionized distilled water, amounting to three microliters each, were carefully dispensed onto the sample surface employing the sessile drop measurement method. Three distinct measurements were carried out for each specimen to ensure accuracy and reliability of the results.

Tensile properties were assessed at 23 °C and 50% RH utilizing an Instron 4465 universal testing equipment (Instron Corp., High Wycombe, England) equipped with a 100 N load cell. The initial grip distance was set at 50 mm, and the rate of grip separation was maintained at 1 mm/min. Six specimens of each film, with a width of 6 mm and a length of 75 mm, were measured. Key tensile characteristics, including tensile stress at maximum load, tensile strain (extension) at break (standard), and elastic modulus (E-modulus), were meticulously determined for each film.

The surface structure of the film was examined using scanning electron microscopy (SEM) equipped with an X-ray analyzing system (Thermo Scientific, Germany). Comprehensive images were captured from both sides of the film at various magnifications, providing a detailed analysis of the surface morphology. Additionally, the cross-section of the broken film was subjected to thorough examination for a more in-depth understanding of the film's internal structure.

Fourier transform infrared (FTIR) spectroscopy of the films was conducted using a Thermo Scientific Nicolet iS™ 50 FTIR spectrometer (USA). The spectra were acquired through 64 scans with a resolution of 4 cm^{-1} within the wavenumber range of 4000–400 cm^{-1}.

3. Results and discussion

3.1. Raw material characterization

The characterization of discarded carrot pulp was previously detailed in our earlier work [4]. The moisture content was 89.70 ± 1.56% (w/w). with the remaining components presented on a dry basis. Notably, water extractives constituted 63.87 ± 1.28% (w/w), hexane extractives were 1.20 ± 0.79% (w/w), cellulose 10.71 ± 0.40% (w/w), arabinogalactan hemicellulose 8.43 ± 0.02% (w/w), homogalacturonan pectin 5.78 ± 0.34% (w/w), lignin 7.75 ± 0.24% (w/w), and proteins 2.26 ± 0.44% (w/w). The high content of extractives will be a challenge for the subsequent purification of the extracted polymers during the hydrolysis.

3.2. Hydrothermal extracts characterization

The chemical characterization of the three hydrothermal extracts (E1, E2 and E3) is detailed in Table 2, revealing distinct composition profiles influenced by operational parameters. Extraction using a single reactor (E1) produced a less concentrated extract compared to E2 and E3. Across all extracts, free sugars dominated, with sucrose as the most abundant, followed by glucose and fructose. Notably, the E2 extraction, employing seven reactors, exhibited a sevenfold increase in free sugars compared to E1 (12.098 g/L vs. 1.765 g/L). The concurrent increase in reactor count and free sugar concentration underscores the consistent efficiency of the extraction process, demonstrating that the efficiency is preserved when transitioning from the use of a single reactor to multiple reactors operating in sequence.

Table 2
Chemical composition of the hydrothermal extract E1 (140 °C, 25 min, 1 reactor), E2 (140 °C, 45 min/reactor, 7 reactors, total 150 min), and E3 (180 °C, 30 min/reactor, 7 reactors, total 100 min).

	E1	E2	E3
Biopolymers (g/L)	**0.882**	**3.894**	**4.363**
Galacto- (g/L)	0.356	1.791	3.164
Arabino- (g/L)	0.237	0.996	0.606
Arabinogalactan (g/L)	0.593	2.787	3.770
Homogalacturonan (g/L)	0.290	1.108	0.593
AG/(AG+P)	0.672	0.716	0.864
Free sugars (g/L)	**1.765**	**12.098**	**21.819**
Sucrose (g/L)	0.820	6.072	9.739
Glucose (g/L)	0.483	3.286	7.399
Fructose (g/L)	0.462	2.740	4.681
By-products (g/L)	**0.176**	**0.603**	**3.051**
Arabinose (mg/L)	21.9	n.d.	1522.74
Glycolaldehyde (mg/L)	32.2	n.d.	405.35
Formic acid (mg/L)	30.7	363.31	472.79
Acetic acid (mg/L)	41.6	196.12	281.00
Levulinic acid (mg/L)	1.9	n.d.	n.d.
Acrylic acid (mg/L)	45.3	14.4	253.58
5-HMF (mg/L)	1.8	28.9	109.28
Furfural (mg/L)	n.d.	n.d.	5.7

AG: arabinogalactan, P: pectin, 5-HMF: 5-(hydroxymethyl)furfural

In E3, conducted at 180 °C, the sugar content nearly doubled compared to 140 °C, despite a shorter operation time (21.819 g/L vs. 12.098 g/L, 30 min vs. 45 min). This may result not only from the correlation between increased temperature and improved extraction of free sugars; it also stems from the extended time required to reach 180 °C compared to 140 °C. During preheating the raw material is already loaded into the reactors and the extraction of free sugars would begin. The effect of preheating time would affect more when operating with a larger number of reactors.

Arabinogalactan was the predominant biopolymer in all cases, followed by homogalacturonan. The AG/(AG+P) ratio in E1 and E2 was similar (0.672 vs. 0.716), while E3 exhibited a higher ratio (0.864) attributed to lower pectin concentration (0.593 g/L vs. 1.108 g/L). This could stem from prolonged pectin required extraction time or homogalaturonan degradation at high temperatures.

Degradation can be seen in the concentration of arabinan, which was much lower in E3 than in E2 (0.606 g/L vs. 0.996 g/L). This is because arabinose is part of the shorter arabinogalactan chains and is therefore the component most easily released on autohydrolysis. This can be confirmed by the presence of arabinose monomer units in the E3 extract (1522.74 mg/L), which are not present in E2. The content of by-products was low compared to free sugars and biopolymers, although it was markedly higher operating at the higher temperature (3.051 g/L in E3 vs. 0.603 g/L in E2). These by-products would come from the temperature degradation of the sugars.

The molecular weight distribution in Fig. 2 aligns with the composition results. Peaks associated with monomers (glucose, fructose, arabinose) and dimers (sucrose) are evident, along with a broad distribution of arabinogalactan and homogalacturonan, yielding high polydispersity indexes (PDs): 31.6 (E1), 19.2 (E2), and 18.2 (E3). Despite moderate weight-average molecular weights (MW) (18.83 kDa for E1, 14.77 kDa for E2, and 8.08 kDa for E3), semicontinuous hydrothermal treatment successfully extracted very high molecular weight biopolymers. This was due to a reduced autohydrolysis phenomenon due to the low residence time of the liquid in the reactor (about 7 min in all cases). The need for fractionation arises from the broad distribution and substantial presence of high molecular weight biopolymers. Purified and narrow fractions are crucial for downstream processing, such as film production, ensuring optimal material characteristics. The results emphasize the intricate interplay of temperature, time, and reactor configuration in shaping extract composition and molecular weight distribution, vital for targeted biopolymer valorization.

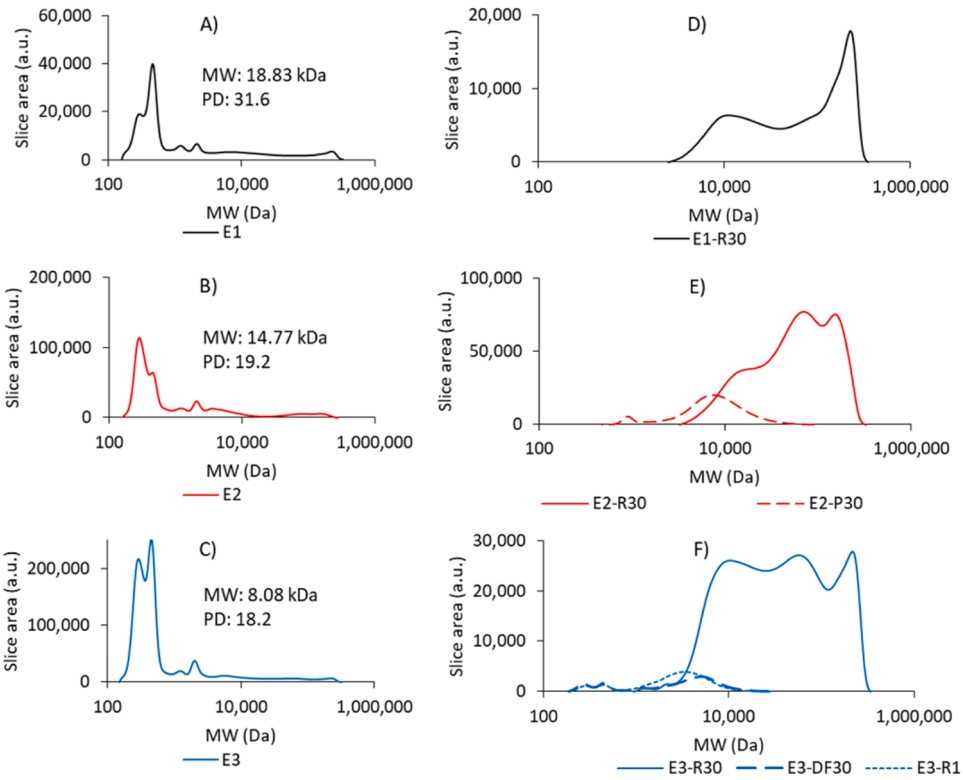

Fig. 2. Molecular weight distribution of the hydrothermal extracts (E1, E2 and E3) and the purified pectin-containing hemicellulose samples.

3.3. Characterization of the purified pectin-containing hemicellulose samples from the ultrafiltration and diafiltration

The purified fractions obtained through multiple UF/DF stages (Fig. 1) underwent comprehensive characterization, as detailed in Table 3. The fractions exhibited a diverse MW range, encompassing products ranging from 3.48 kDa to 102.75 kDa. Notably, the PDs remained consistently low, ranging from 2.1 to 4.0, indicating the suitability of these fractions for various applications. The results affirm the efficacy of the fractionation process in producing distinct biopolymer subsets with desirable characteristics.

Examining the higher molecular weight fractions, E1-R30, derived from a single reactor extraction, exhibited the lowest concentration (2.89 g/L biopolymers). In contrast, E2-R30 demonstrated significantly higher concentration (19.3 g/L biopolymers), owing to the optimal extraction temperature (140 °C) for high molecular weights and the application of UF with the 10 kDa and 30 kDa membranes. E3-R30, with a concentration of 6.91 g/L biopolymers, faced higher autohydrolysis effects and utilized DF without UF with the 30 kDa membrane (Fig. 1). The intermediate and low MW fractions exhibited lower concentration than their high MW counterparts.

A remarkable outcome of the fractionation process was the near-total elimination of free sugars and by-products in higher MW fractions (> 4.03 kDa), achieving purities between 98.89–100% (w/w). However, lower MW fractions (E3-DF30, E3-R1) demonstrated lower purities (65.08 and 66.67% w/w), necessitating a higher number of DF cycles on the lower MWCO membrane. The AG/(AG+P) values, representing the proportion of arabinogalactan to pectin, showed variability (0.58–0.90), seemingly unrelated to MW. The proportion of galactan in arabinogalactan was consistent across all samples (0.62–0.65), slightly lower in lower MW samples like E2-P30 and E3-R1 (0.58, 0.57).

Distinct molecular weight distributions emerged in the six fractionated samples after UF/DF, illustrated in Figs. 2D, 2E, and 2F. E1-R30 exhibited a distinctive high molecular weight peak (100–225 kDa), also present in E2-R30 and E3-R30. In E2-R30 and E3-R30, a secondary lower molecular weight peak (50–70 kDa) became prominent, likely due to extended reaction times and higher temperature inducing greater autohydrolyis. A third lower MW peak (approx. 10 kDa) appeared in all three fractions, suggesting direct extraction from the solid rather than a product of already extracted biopolymers. This was previously demonstrated [4]. E2-P30 featured a narrower, less concentrated, and lower molecular weight distribution. Samples E3-DF30 and E3-R1, with lower concentration and purity (65.08–66.67%), displayed the presence of peaks associated with monosaccharides and disaccharides in their distributions.

Table 3
Characterization of the purified pectin-containing hemicellulose samples from the ultrafiltration and diafiltration of extract E1, E2 and E3.

	MW (kDa)	PD	AG (g/L)	Pectin (g/L)	Free sugars (g/L)	Byproducts (g/L)	Biopolymers (% w/w)	AG/(AG+P)	G/(A+G)
E1-R30	102.75	4.0	1.69	1.20	n.d.	0.03	98.89%	0.58	0.64
E2-R30	80.36	2.4	17.38	1.92	n.d.	n.d.	100%	0.90	0.65
E2-P30	9.85	2.1	1.14	1.21	n.d.	n.d.	100%	0.49	0.58
E3-R30	67.77	3.8	5.06	1.85	n.d.	n.d.	100%	0.73	0.62
E3-DF30	4.03	3.5	0.33	0.08	0.22	n.d.	65.08%	0.80	0.63
E3-R1	3.48	2.5	0.97	0.57	0.73	0.04	66.67%	0.63	0.57

MW: weight-average molecular weight, PD: polydispersity index, AG: arabinogalactan, P: pectin, G: galactan, A: arabinan

3.4. Characterization of the residual pulp and lignin-containing cellulose nanofibers

The freeze-dried residual pulp from one of the reactors of E2 extraction process was thoroughly characterized on a dry basis. Cellulose emerged as the predominant compound, constituting 34.68 ± 3.91% (w/w), followed by lignin at 21.04 ± 3.66% (w/w). This composition positions the material as a promising candidate to produce cellulose nanofibers enriched with lignin. The contents of arabinogalactan hemicellulose and homogalacturonan pectin were measured at 3.43 ± 1.27% (w/w) and 1.07 ± 0.26% (w/w), respectively. Despite these promising attributes, a notable proportion of water extractives (> 20% w/w) persisted in the residual pulp, suggesting that an extended extraction time or higher temperature might further reduce this component.

The freeze-dried residual pulp underwent ball milling and high-pressure homogenization to yield a suspension of L-CNFs. Prior to homogenization, optical microscope images (Figure A.1) revealed the presence of aggregates in the suspension of milled residual pulp, varying in morphology and reaching sizes up to 300 μm. However, after high-pressure homogenization, these aggregates were no longer observed, indicating a homogenous distribution. Similarly, TEM analysis (Fig. 3) initially revealed fiber aggregates within the 50–300 μm size range (before the homogenization). After processing, the fibers were observed in a more isolated form, featuring lower diameters, between 10–15 nm, and lengths exceeding 1 μm. The presence of lignin was also apparent in the fibers in the form of nanometer-sized granules, particularly before homogenization. Post-homogenization, lignin exhibited in a more uniform distribution.

3.5. Film based on pectin-containing arabinogalactan versus film based on lignin-containing cellulose nanofibers

As shown in Table 1, films A and Z were based on two distinct fractions resulting from the hydrothermal treatment applied to discarded carrot pulp, i.e.: pectin-containing arabinogalactan and lignin-cellulose nanofibers, respectively. For the preparation of film A, based on P-AG, the purified sample E3-R30 was used, and its characterization is detailed in Table 3. Film Z, on the other hand, was made from the L-CNFs sample obtained through the physical treatment applied to the residual pulp from extraction E2, and its characterization is explained in Section 3.4. All films, including A and Z, featured a 35% (w/w) content of glycerol as plasticizing agent.

Fig. 4 presents the characterization of these films based on their barrier properties (OP and WVP), surface hydrophobicity (water contact angle), and mechanical properties (tensile strength, elongation, and elastic modulus).

The barrier properties of the prepared films aligned with the general trend that hemicelluloses and pectins exhibit robust oxygen barrier capabilities but are comparatively less effective against water vapor. Film Z demonstrated a 71.8% lower OP compared to film A (67.73 vs. 239.83 $cm^3STP \cdot \mu m/m^{2/}kPa/day$), underscoring that the P-AG sample is more adept at minimizing OP than the L-CNFs fraction. Regarding water vapor barrier performance, both films exhibited nearly identical WVP values ($2.06 \cdot 10^{-10}$ for film A vs. $2.04 \cdot 10^{-10}$ $g \cdot m/m^2/s/Pa$ for film Z).

The surface hydrophobicity, evaluated on the rougher top side of the films (the side exposed to air during drying), revealed distinct characteristics. The difference between the top and bottom sides of the films, as well as the cross section, can be seen in the Supplementary Information. Films A and Z displayed contact angles of 79.9° and 87.9°, respectively. A contact angle exceeding 90° is typically indicative of a hydrophobic surface, categorizing film Z as almost hydrophobic, in contrast to the more hydrophilic character of the P-AG film. This discrepancy may be attributed to the presence of lignin in the film Z, the sole hydrophobic biopolymer among those used.

Regarding the mechanical properties, film Z, based on L-CNFs, exhibited a tensile strength 146.6% higher than film A, based on P-AG (7.74 vs. 3.14 MPa). This difference may be attributed to the inherently higher tensile strength associated with cellulose compared to other biopolymers. However, film A displayed an elongation percentage 25.8% higher than film Z (12.49 vs. 9.93%), possibly due to the greater stretchability of arabinogalactan hemicellulose compared to cellulose or lignin. The elastic modulus was 46.1% higher in film Z than in film A (158.76 vs. 85.57 MPa), indicating that the L-CNFs-based film was stiffer than the P-AG-based film. The stress-strain curves of the films can be seen in the Supplementary Information (Figure A.5). This comprehensive analysis sheds light on the diverse properties and characteristics of the films, offering insights into their potential applications and highlighting the nuanced interplay between different biopolymers in influencing film properties.

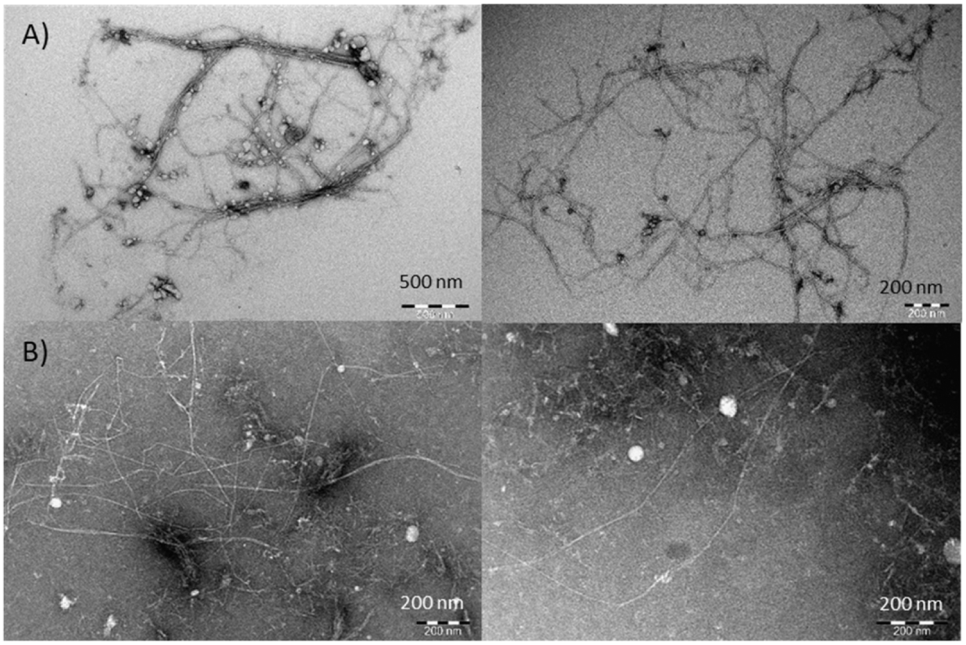

Fig. 3. TEM images of L-CNFs from discarded carrot pulp (A) before homogenization, and (B) after homogenization.

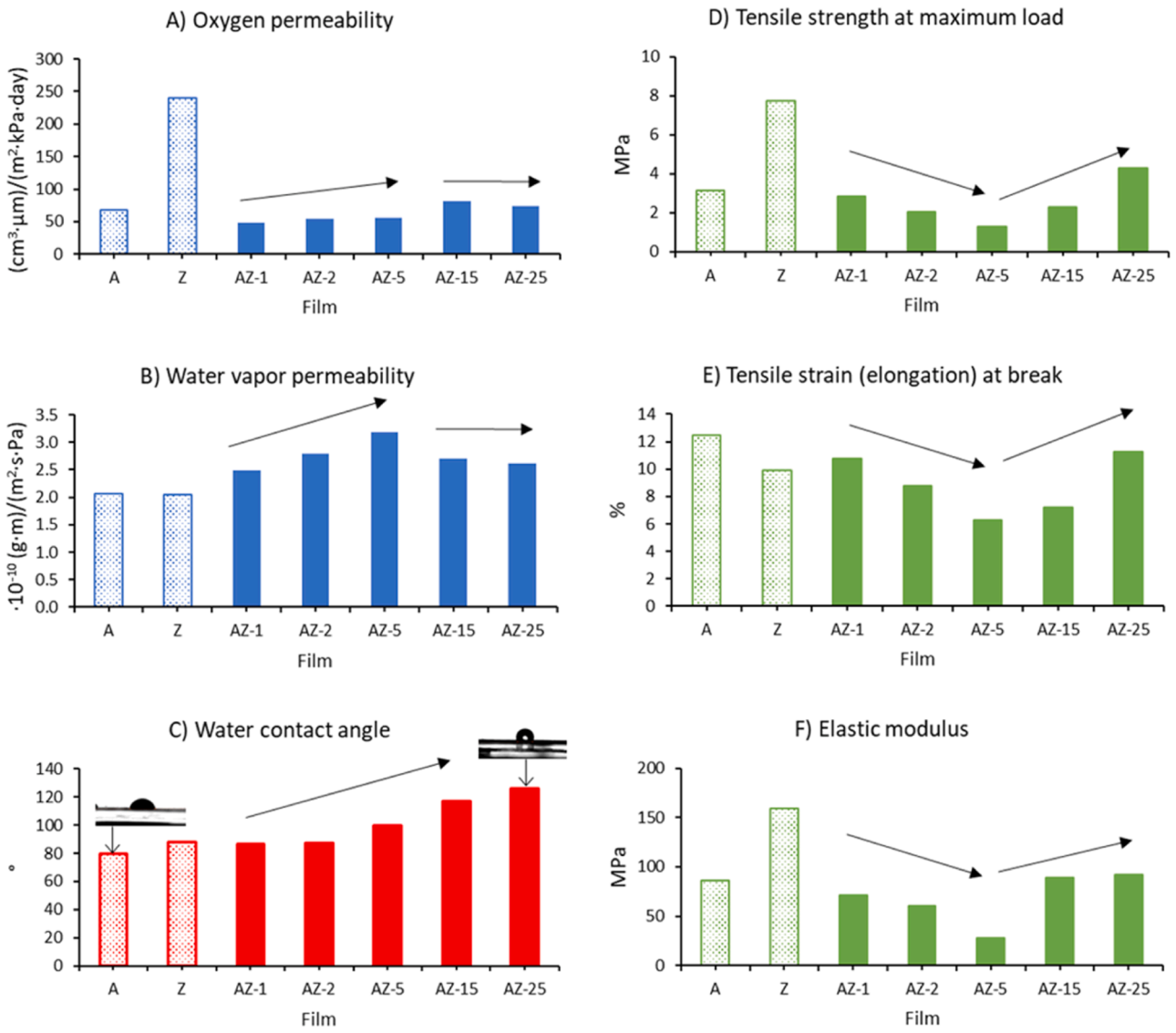

Fig. 4. Oxygen permeability, water vapor permeability, water contact angle, and mechanical properties of the films A (65% P-AG), Z (65% L-CNFs), AZ-1 (64% P-AG, 1% L-CNFs), AZ-2 (63% P-AG, 2% L-CNFs), AZ-5 (60% P-AG, 5% L-CNFs), AZ-15 (50% P-AG, 15% L-CNFs), and AZ-25 (40% P-AG, 25% L-CNFs).

3.6. Films based on the combination of pectin-containing arabinogalactan and lignin-cellulose nanofibers

To explore potential synergistic properties of both biopolymer samples, mixed films were prepared based on the P-AG fraction, incorporating varying percentages of the L-CNFs fraction (1, 2, 5, 15, and 25% w/w). Supplementary Information (Figure A.3) provides images of the films, and Fig. 4 displays the permeability values for oxygen and water vapor. The increase of L-CNFs from 1 to 5% (films AZ-1, AZ-2, and AZ-5) resulted in an increase in the permeabilities, indicating that a small percentage addition of this fraction was not beneficial. However, at higher content, as in AZ-15 and AZ-25 films (15 and 25%, respectively), permeability values approached those of the reference film A, based on P-AG. Two trends were observed, with the presence of L-CNFs not being beneficial initially, potentially due to a reduction in the percentage of AG-P without compensatory benefits from these fibers.

However, beyond a certain percentage, L-CNFs compensated for the absence of AG-P, leading to improved permeability values. Similar findings were reported by Hu et al. (2016), where the addition of CNFs exhibited two trends: 10% CNFs increased the WVTR value from 45.7 to 74.6 g/m^2·h, while the addition of 20 and 30% CNFs decreased the WVTR value to 43.8 and 35.4 g/m^2·h [31]. The addition of higher CNFs content favored the presence of more structured layers in the material, reducing permeability.

Concerning surface hydrophobicity, a synergistic effect was observed between the two fractions. While the hydrophobicity of films A and Z did not differ significantly, the mixing of the two fractions increased hydrophobicity as the L-CNFs content increased. The AZ-25 film demonstrated the most hydrophobic surface, with a contact angle of 125.8°, 57.5% higher than the P-AG-based film. This synergistic effect could be associated with the rough morphology of the film surface when both fractions are mixed, as depicted in Figure A.2.

Mechanical properties, as shown in Fig. 4, displayed two distinct regions of behavior. L-CNFs in percentages lower than 5% (AZ-1, AZ-2, and AZ-5) were not beneficial, as the mechanical properties were inferior to those of the reference films (A and Z). At low L-CNFs content, the P-AG fraction dominated, with the addition of L-CNFs acting as more of a defect than a benefit. In the AZ-5 film (5% L-CNFs), the tensile strength decreased by 59.5% compared to the A film (1.27 vs. 3.14 MPa) and the elongation decreased by 49.6% (6.29 vs. 12.49%). However, higher L-CNFs content, as in AZ-15 (15%) and AZ-25 (25%), resulted in improved mechanical properties, approaching values similar to those of the

reference films (A and Z). The AZ-25 film exhibited a tensile strength of 4.31 MPa, elongation of 11.27%, and an elastic modulus of 92.23 MPa. Comparing with the literature, Liu et al. (2016) combined hemicelluloses and chitosan to make films, and achieved a tensile strength value of 14.26 MPa, higher than in the present work [32]. By reinforcing the hemicellulose/chitosan films with CNFs, Xu et al. (2019b) obtained a tensile stress between 31.02 – 38.56 MPa and elongation between 10.07 – 15.98% [33]. The lower strength of the films in the present work could be associated with the arabinogalactan hemicellulose, which in previous studies has given rise to the most brittle films in comparison to other hemicelluloses [20]. The two regions observed in the tensile properties concerning fibers content align with findings from Ryu and Lee (2001), who observed that at low fibers percentages (< 15%), tensile strength was dominated by the main biopolymer, with fibers acting as a network defect due to the high difference in their moduli [34]. Beyond a critical fibers content, tensile strength began to be dominated by the fibers, resulting in increased values.

The comparison of our films with those based on traditional CNFs reveals notable differences. In the studies by Alves et al., CNFs were obtained by different methods and incorporated into composite films by the addition of clay minerals [35,36]. The mechanical properties of their films exceeded those of the present work, albeit with comparable elongation. While the present films exhibited a lower OTR compared to certain composite films, the values were higher than those of the film composed solely of CNFs. The OTR for their films ranged from 1–10000 $cm^3/m^2/d$, while the present work showed values between 7.44–83.28 $cm^3/m^2/d$. The present WVTR was within the range of 249.6–375.2 $g/m^2/d$, while their values were in the range of 100–320 $g/m^2/d$. The films could therefore be comparable in barrier properties, but would need improvement to achieve such mechanical properties.

3.7. Films with different pectin-containing arabinogalactan samples

As can be seen in Table 1, six films with six distinct P-AG samples were prepared, each containing 1% (w/w) L-CNFs to emphasize the influence of the P-AG fraction. Images of the films can be seen in Figure A.6 and the FTIR results are also commented in the Supplementary Information (Figure A.7). The films made with the three lower molecular weight samples, DZ-1, EZ-1 and FZ-1 films, proved too brittle and broke upon retrieval from the Petri dish, preventing sufficient quality characterization. The brittleness could be attributed to the low

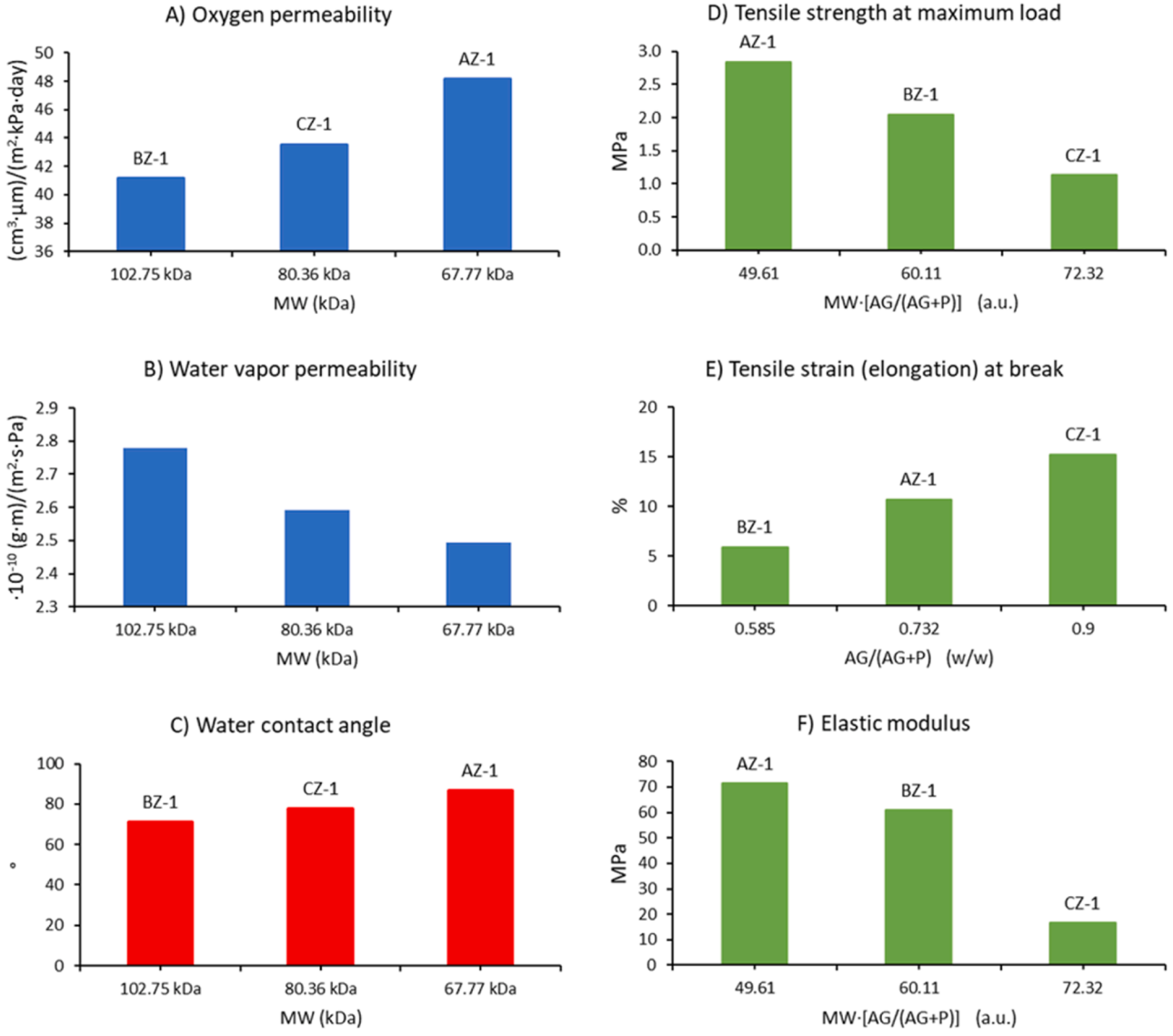

Fig. 5. Oxygen permeability, water vapor permeability, water contact angle, and mechanical properties of the films BZ-1 (102.75 kDa, AG/(AG+P)=0.585), CZ-1 (80.36 kDa, AG/(AG+P)=0.900), and AZ-1 (67.77 kDa, AG/(AG+P)=0.732).

molecular weight of the P-AG fractions (max. 9.85 kDa) and lower purity in some cases (65.08% w/w in E3-DF30, film EZ-1, and 66.67% w/w in E3-R1, film FZ-1). In contrast, the other three films (AZ-1, BZ-1, and CZ-1) were successfully prepared with P-AG fractions of very high molecular weight (min. 67.77 kDa) and purities of at least 98.89% (w/w). These films remained intact and were characterized to study the combined effects of molecular weight and the proportion of arabinogalactan and pectin. As there were no groups of films with the same molecular weight and different composition or vice versa, the study of these properties needed to be conducted jointly.

Fig. 5 shows the properties of the films concerning the fraction of P-AG used. Regarding barrier properties, distinct behaviors were observed. OP decreased by up to 14.6% with increasing molecular weight (41.14 vs. 48.18 $cm^3STP{\cdot}\mu m/m^2/kPa/day$), likely due to a greater number of bonds creating more tortuous pathways for oxygen, thereby reducing permeability. The OP values were comparable to conventional petroleum-based plastics such as polyethylene terephthalate (10–50 $cm^3{\cdot}\mu m/m^2/kPa/day$) and lower than polypropylene (100–500 $cm^3{\cdot}\mu m/m^2/kPa/day$) [37]. Previous studies have also found that a higher molecular weight decreases OP [38]. In contrast, WVP increased by up to 11.4% with an increase in molecular weight ($2.78{\cdot}10^{-10}$ vs. $2.49{\cdot}10^{-10}$ $g{\cdot}m/m^2/s/Pa$). This elevation could be attributed to the hydrophilic nature of both arabinogalactan and pectin, unable to hinder water vapor passage despite an increased number of bonded monomers in the structure. Surface hydrophobicity decreased by up to 18.13% with higher molecular weight (71.10° vs. 86.84°), possibly due to changes in the interaction between functional groups of P-AG and L-CNFs. As seen in Fig. 4, higher hydrophobicity resulted from a synergistic effect between the two fractions. A higher molecular weight of the P-AG fraction might lead to lower interaction between the functional groups of P-AG and L-CNFs, resulting in reduced hydrophobicity.

The study of mechanical properties for films BZ-1, CZ-1 and AZ-1 involved determining stress-strain curves, as despicted in the Supplementary Information (Figure A.8). Parameters characterizing mechanical behavior were derived from these curves. The analysis revealed that not only the molecular weight but also composition, understood as the greater or lesser proportion of arabinogalactan and pectins, played a crucial role. Fig. 5 plots tensile strength against the product of MW and the ratio of arabinogalactan to total arabinogalactan and pectins (AG/(AG+P)). This suggests that lower molecular weight has a comparable effect to a higher pectin content regarding arabinogalactan content. Despite CZ-1 film having a higher molecular weight, the AZ-1 film exhibited the highest tensile strength, 150.9% higher than CZ-1 film (2.835 vs. 1.130 MPa). This phenomenon is attributed to the peculiarities of arabinogalactan hemicellulose. As demonstrated in previous studies, a higher presence of arabinogalactan does not necessarily improve the mechanical strength due to the more contents of side chains disturbing the arrangements [25].

Concerning the elongation of the films, no remarkable dependence was found on molecular weight, but a significant correlation was observed with the composition of the films. Higher arabinogalactan content relative to pectin content resulted in films with higher elongation. For instance, CZ-1 was 157.9% more stretchable than BZ-1 (15.275 vs. 5.923%). The elastic modulus depended on both molecular weight and greater or lesser presence of arabinogalactan or pectins. As shown in Fig. 5, films were more elastic (lower modulus) for higher molecular weight and a higher presence of arabinogalactan, while they were stiffer for lower molecular weight and a higher presence of pectins. Consequently, the elastic modulus of the AZ-1 film was 332.1% higher than that of the CZ-1 film (71.315 vs. 16.505 MPa). From a tensile perspective, if a film with higher strength is sought after, the lowest molecular weight still sufficient to form the film would be the best choice, along with the highest possible pectin content. For a film with higher stretchability, a high arabinogalactan content should be beneficial. Previous work combining hemicelluloses (arabinoxylan), pectins, and 25% (w/w) commercial cellulose nanocrystals (CNCs) to produce films also found that hemicelluloses increased elongation over pectins (12.99 vs. 4.73%), while pectins increased tensile strength over hemicelluloses (68.93 vs. 2.73 MPa) [27]. The study of these properties allows for a nuanced understanding of how different factors contribute to the final film characteristics and provides a basis for optimizing film properties based on the desired application.

In terms of economic feasibility, the present study investigates various steps, including extraction, separation, purification and drying (arabinogalactan and pectins), as well as extraction, drying, ball milling, and high pressure homogenization (L-CNFs). The inclusion of numerous stages stems from the objective of optimizing the raw material for film manufacturing. It would be more technically and economically viable to produce films based on either of the two fractions. For films based on arabinogalactan and pectins, the ball milling and homogenization steps could be omitted, just as for the manufacture of films based on L-CNFs, where separation and purification steps are unnecessary. Regarding the extraction of arabinogalactan and pectins, the hydrothermal extraction step proves advantageous from a feasibility standpoint due to the use of water as the sole reagent and the incorporation of an energy integration system that allows heating part of the inlet stream with the outlet stream, as shown in our previous work [17]. Concerning the separation and purification of arabinogalactan and pectins, the use of UF membranes requires only the application of pressure (2–3.5 bar) through a pump and water for DF, making it a more economical process compared to alternatives such as separation with organic solvents or chromatography. It is worth noting that the drying stage of the biopolymers, achieved through spray drying or freeze drying, was only conducted for storage, characterization, and film elaboration in different proportions. Consequently, this step could be omitted, and since the biopolymers are purified, films could be directly formed from the liquid product obtained after UF and DF, with the addition of the corresponding plasticizing agent. For large-scale film production, initiating the process with a powder or a highly concentrated solution (potentially achieved through vacuum evaporation) facilitates extrusion. However, the extrusion technique fall beyond the parameters of this study.

4. Conclusions

Discarded carrots were successfully valorized through subcritical hydrolysis, yielding biopolymeric fractions to produce bio-based films. Pectin-containing arabinogalactan (P-AG) extracted via hydrothermal treatment was purified through multiple cycles of UF and DF, resulting in solid fractions of molecular weights ranging from 3.48 to 102.75 kDa, whereas the extracts were 8.08–18.83 kDa. Simultaneously, lignin-containing cellulose nanofibers (L-CNFs) were derived from the residual solid obtained after the hydrothermal treatment through mechanical treatments. Films were produced from both fractions, with the P-AG film exhibiting superior oxygen barrier characteristics, while the L-CNFs film demonstrated higher tensile strength. Further exploration involved the formulation of films based on P-AG with varying percentages of added L-CNFs. L-CNFs proved beneficial only when their percentage exceeded 15% (w/w), acting as enhancements rather than defects. The synergistic effect between both fractions contributed to improved hydrophobicity, reaching a notable water contact angle of 125.8°. Diversifying the study, different purified P-AG samples were utilized to create films. Higher molecular weight correlated with decreased OP, increased WVP, and slightly reduction in hydrophobicity. Additionally, tensile strength exhibited an inverse relationship with molecular weight, emphasizing the unique mechanical properties of branched arabinogalactan. Higher pectin content corresponded to increased tensile strength while higher arabinogalactan content correlated with increased elongation. The films were produced from a novel raw material and distinct fractions and demonstrated acceptable properties, showcasing the potential for sustainable alternatives in food packaging. Subsequent evaluation of biodegradability and the incorporation of smart properties (e.g.,

antioxidant or antibacterial capacity) will enable their broader application.

CRediT authorship contribution statement

Marta Ramos-Andrés: Writing – review & editing, Writing – original draft, Visualization, Validation, Methodology, Investigation, Formal analysis, Data curation, Conceptualization. **Chunlin Xu:** Writing – original draft, Visualization, Supervision, Project administration, Conceptualization. **Juan García-Serna:** Writing – review & editing, Writing – original draft, Visualization, Supervision, Project administration, Conceptualization. **Liqiu Hu:** Writing – original draft, Methodology, Investigation. **Henrik Grénman:** Writing – original draft, Supervision, Conceptualization.

Declaration of Competing Interest

The authors declare that they have no known competing financial interests or personal relationships that could have appeared to influence the work reported in this paper.

Data Availability

The data of the present research is available for use by researchers in the official public repository of the University of Valladolid at the following link: https://uvadoc.uva.es/handle/10324/62681

Acknowledgments

This work was supported by the Agencia Estatal de Investigación (Gobierno de España) and FEDER Funds EU [PID2019–105975GB-I00 (MICINN/FEDER, EU)]; and Junta de Castilla y León - Consejería de Educación and FEDER Funds [CLU-2019–04]. PhD. Marta Ramos-Andrés wishes to thank the Spanish Ministry of Education, Culture and Sports for the research-university professor training contract [FPU15/06366], and the Johan Gadolin Process Chemistry Centre (PCC) for the International Mobility grant. Mr. Liqiu Hu would like to acknowledge the financial support from the China Scholarship Council [Student ID 201908120107]. The authors wish also to thank the company Muñozval S.L. for the raw material supply and the advice, and Rajesh for the guidance on OTR and WVTR measurements.

Appendix A. Supporting information

Supplementary data associated with this article can be found in the online version at doi:10.1016/j.jece.2024.112645.

References

[1] A.M.I. Encalada, C.D. Pérez, S.K. Flores, L. Rossetti, E.N. Fissore, A.M. Rojas, Antioxidant pectin enriched fractions obtained from discarded carrots (Daucus carota L.) by ultrasound-enzyme assisted extraction, Food Chem. 289 (2019) 453–460, https://doi.org/10.1016/j.foodchem.2019.03.078.
[2] M. Marić, A.N. Grassino, Z. Zhu, F.J. Barba, M. Brnčić, S. Rimac Brnčić, An overview of the traditional and innovative approaches for pectin extraction from plant food wastes and by-products: ultrasound-, microwaves-, and enzyme-assisted extraction, Trends Food Sci. Technol. 76 (2018) 28–37, https://doi.org/10.1016/j.tifs.2018.03.022.
[3] S. Varanasi, L. Henzel, S. Sharman, W. Batchelor, G. Garnier, Producing nanofibres from carrots with a chemical-free process, Carbohydr. Polym. 184 (2018) 307–314, https://doi.org/10.1016/j.carbpol.2017.12.056.
[4] M. Ramos-Andrés, B. Aguilera-Torre, J. García-Serna, Hydrothermal production of high-molecular weight hemicellulose-pectin, free sugars and residual cellulose pulp from discarded carrots, J. Clean. Prod. (2020) 125179, https://doi.org/10.1016/j.jclepro.2020.125179.
[5] N.R. Aimaretti, C.V. Ybalo, M.L. Rojas, F.J. Plou, J.C. Yori, Production of bioethanol from carrot discards, Bioresour. Technol. 123 (2012) 727–732, https://doi.org/10.1016/j.biortech.2012.08.035.
[6] A.L. Clementz, D. Manuale, E. Sanchez, C. Vera, J.C. Yori, Use of discards of bovine bone, yeast and carrots for producing second generation bio-ethanol, Biocatal. Agric. Biotechnol. 22 (2019) 101392, https://doi.org/10.1016/j.bcab.2019.101392.
[7] J.C. López-Linares, A. Mateo Martínez, M. Coca, S. Lucas, M.T. García-Cubero, Carrot Discard as a Promising Feedstock to Produce 2, 3-Butanediol by Fermentation with P. polymyxa DSM 365, (2023).
[8] J.C. López-Linares, M. Coca, P.E. Plaza, S. Lucas, M.T. García-Cubero, Waste-to-fuel technologies for the bioconversion of carrot discards into biobutanol, Renew. Energy 202 (2023) 362–369, https://doi.org/10.1016/j.renene.2022.11.093.
[9] A. Elik, D.K. Yanık, F. Göğüş, Microwave-assisted extraction of carotenoids from carrot juice processing waste using flaxseed oil as a solvent, Lwt 123 (2020), https://doi.org/10.1016/j.lwt.2020.109100.
[10] A. Clementz, P.A. Torresi, J.S. Molli, D. Cardell, E. Mammarella, J.C. Yori, Novel method for valorization of by-products from carrot discards, Lwt 100 (2019) 374–380, https://doi.org/10.1016/j.lwt.2018.10.085.
[11] L. Salvañal, A. Clementz, L. Guerra, J.C. Yori, D. Romanini, L-lactic acid production using the syrup obtained in biorefinery of carrot discards, Food Bioprod. Process. 127 (2021) 465–471, https://doi.org/10.1016/j.fbp.2021.04.002.
[12] A.M. Idrovo Encalada, M.F. Basanta, E.N. Fissore, M.D. De'Nobili, A.M. Rojas, Carrot fiber (CF) composite films for antioxidant preservation: Particle size effect, Carbohydr. Polym. 136 (2016) 1041–1051, https://doi.org/10.1016/j.carbpol.2015.09.109.
[13] L. Amoroso, K.J. De France, C.I. Milz, G. Siqueira, T. Zimmermann, G. Nyström, Sustainable cellulose nanofiber films from carrot pomace as sprayable coatings for food packaging applications, ACS Sustain. Chem. Eng. 10 (2022) 342–352, https://doi.org/10.1021/acssuschemeng.1c06345.
[14] G. Perotto, R. Simonutti, L. Ceseracciu, M. Mauri, D. Besghini, A. Athanassiou, Water-induced plasticization in vegetable-based bioplastic films: A structural and thermo-mechanical study, Polym. (Guildf.) 200 (2020) 122598, https://doi.org/10.1016/j.polymer.2020.122598.
[15] E. Sogut, H. Cakmak, Utilization of carrot (Daucus carota L.) fiber as a filler for chitosan based films, Food Hydrocoll. 106 (2020), https://doi.org/10.1016/j.foodhyd.2020.105861.
[16] M. Ramos-Andrés, B. Aguilera-Torre, J. García-Serna, Biorefinery of discarded carrot juice to produce carotenoids and fermentation products, J. Clean. Prod. 323 (2021) 129139, https://doi.org/10.1016/j.jclepro.2021.129139.
[17] M. Ramos-Andrés, S. Díaz-Cesteros, N. Majithia, J. García-Serna, Pilot-scale biorefinery for the production of purified biopolymers based on hydrothermal treatment in flow-through reactor cycles, Chem. Eng. J. 437 (2022), https://doi.org/10.1016/j.cej.2022.135123.
[18] P. Immerzeel, M.M. Eppink, S.C. De Vries, H.A. Schols, A.G.J. Voragen, Carrot arabinogalactan proteins are interlinked with pectins, Physiol. Plant. 128 (2006) 18–28, https://doi.org/10.1111/j.1399-3054.2006.00712.x.
[19] M. Ramos-Andrés, B. Aguilera-Torre, J. García-Serna, Production of purified hemicellulose-pectin fractions of different molecular weight from discarded carrots by hydrothermal treatment followed by multistep ultrafiltration/diafiltration, J. Clean. Prod. 321 (2021) 128923, https://doi.org/10.1016/j.jclepro.2021.128923.
[20] F. Peng, P. Peng, F. Xu, R.C. Sun, Fractional purification and bioconversion of hemicelluloses, Biotechnol. Adv. 30 (2012) 879–903, https://doi.org/10.1016/j.biotechadv.2012.01.018.
[21] H. Long, J. Gu, J. Jiang, L. Guan, X. Lin, W. Zhang, C. Hu, Mechanically strong and biodegradable holocellulose films prepared from Camellia oleifera shells, Carbohydr. Polym. 299 (2023) 120189, https://doi.org/10.1016/j.carbpol.2022.120189.
[22] F.R.S. Mendes, M.S.R. Bastos, L.G. Mendes, A.R.A. Silva, F.D. Sousa, A.C. O. Monteiro-Moreira, H.N. Cheng, A. Biswas, R.A. Moreira, Preparation and evaluation of hemicellulose films and their blends, Food Hydrocoll. 70 (2017) 181–190, https://doi.org/10.1016/j.foodhyd.2017.03.037.
[23] R. Gheribi, Y. Habibi, K. Khwaldia, Prickly pear peels as a valuable resource of added-value polysaccharide: study of structural, functional and film forming properties, Int. J. Biol. Macromol. 126 (2019) 238–245, https://doi.org/10.1016/j.ijbiomac.2018.12.228.
[24] N.L. Oliveira, A.A. Rodrigues, I.C. Oliveira Neves, A.M. Teixeira Lago, S.V. Borges, J.V. de Resende, Development and characterization of biodegradable films based on Pereskia aculeata Miller mucilage, Ind. Crops Prod. 130 (2019) 499–510, https://doi.org/10.1016/j.indcrop.2019.01.014.
[25] J. Chen, Y. Ren, W. Liu, T. Wang, F. Chen, Z. Ling, Q. Yong, All-natural and biocompatible cellulose nanocrystals films with tunable supramolecular structure, Int. J. Biol. Macromol. 193 (2021) 1324–1331, https://doi.org/10.1016/j.ijbiomac.2021.10.191.
[26] W. Ren, T. Qiang, L. Chen, Recyclable and biodegradable pectin-based film with high mechanical strength, Food Hydrocoll. 129 (2022) 107643, https://doi.org/10.1016/j.foodhyd.2022.107643.
[27] L.R. Mugwagwa, A.F.A. Chimphango, Physicochemical properties and potential application of hemicellulose/pectin/nanocellulose biocomposites as active packaging for fatty foods, Food Packag. Shelf Life. 31 (2022) 100795, https://doi.org/10.1016/j.fpsl.2021.100795.
[28] B. Chihaoui, Q. Tarrés, M. Delgado-Aguilar, P. Mutjé, S. Boufi, Lignin-containing cellulose fibrils as reinforcement of plasticized PLA biocomposites produced by melt processing using PEG as a carrier, Ind. Crops Prod. 175 (2022), https://doi.org/10.1016/j.indcrop.2021.114287.
[29] J. Trifol, R. Moriana, Barrier packaging solutions from residual biomass: synergetic properties of CNF and LCNF in films, Ind. Crops Prod. 177 (2022) 114493, https://doi.org/10.1016/j.indcrop.2021.114493.
[30] G. Gallina, J. García-Serna, Multi-bed pilot plant and process for biomass fractionation, ES20160031191 20160914, 2018.

[31] S. Hu, J. Gu, F. Jiang, Y.Lo Hsieh, Holistic rice straw nanocellulose and hemicelluloses/lignin composite films, ACS Sustain. Chem. Eng. 4 (2016) 728–737, https://doi.org/10.1021/acssuschemeng.5b00600.
[32] Y. Liu, B. Sun, Z. Wang, Y. Ni, Mechanical and water vapor barrier properties of bagasse hemicellulose-based films, BioResources 11 (2016) 4226–4236, https://doi.org/10.15376/biores.11.2.4226-4236.
[33] J. Xu, R. Xia, L. Zheng, T. Yuan, R. Sun, Plasticized hemicelluloses/chitosan-based edible films reinforced by cellulose nanofiber with enhanced mechanical properties, Carbohydr. Polym. 224 (2019) 115164, https://doi.org/10.1016/j.carbpol.2019.115164.
[34] S.R. Ryu, D.J. Lee, Effects of fiber aspect ratio, fiber content, and bonding agent on tensile and tear properties of short-fiber reinforced rubber, KSME Int. J. 15 (2001) 35–43, https://doi.org/10.1007/BF03184796.
[35] L. Alves, A. Ramos, E. Ferraz, P.J.T. Ferreira, M.G. Rasteiro, J.A.F. Gamelas, Design of cellulose nanofibre-based composites with high barrier properties, Cellulose 30 (2023) 10157–10174, https://doi.org/10.1007/s10570-023-05495-z.
[36] L. Alves, A. Ramos, M.G. Rasteiro, C. Vitorino, E. Ferraz, P.J.T. Ferreira, M. L. Puertas, J.A.F. Gamelas, Composite films of nanofibrillated cellulose with sepiolite: effect of preparation strategy, Coatings 12 (2022) 1–12, https://doi.org/10.3390/coatings12030303.
[37] C. Maes, W. Luyten, G. Herremans, R. Peeters, R. Carleer, M. Buntinx, Recent updates on the barrier properties of ethylene vinyl alcohol copolymer (EVOH): a review, Polym. Rev. 58 (2018) 209–246, https://doi.org/10.1080/15583724.2017.1394323.
[38] M. Chadni, N. Grimi, O. Bals, I. Ziegler-Devin, S. Desobry, N. Brosse, Elaboration of hemicellulose-based films: Impact of the extraction process from spruce wood on the film properties, Carbohydr. Res. 497 (2020), https://doi.org/10.1016/j.carres.2020.108111.